IET Electric Power Applications

Research Article

IET Journals
The Institution of Engineering and Technology

Predictive torque control of open-end winding induction motor drive fed with multilevel inversion using two two-level inverters

ISSN 1751-8660
Received on 26th April 2017
Revised 17th July 2017
Accepted on 2nd August 2017
E-First on 29th September 2017
doi: 10.1049/iet-epa.2017.0209
www.ietdl.org

Kunisetti V. Praveen Kumar[1] ✉, *Thippiripati Vinay Kumar*[1]

[1]*Department of Electrical Engineering, National Institute of Technology Warangal, Warangal, India*

✉ *E-mail: kvpraveenkumar15@gmail.com*

Abstract: This study proposes direct torque and flux control of dual-inverter-fed open-end winding induction motor (OEWIM) with the help of model predictive control. OEWIMs are extensively used in electric vehicles and for ship propulsion but they require a high dynamic performance. Predictive torque control (PTC) retains the features of direct torque control and offers a high dynamic performance by eliminating start-up problems. In this study, predictive torque control is implemented for multilevel inversion-fed OEWIMs. Multilevel inversion is obtained by operating two two-level inverters with equal and unequal DC link voltages. The proposed study gives a comparative analysis of PTC of OEWIM for various speeds and numerical analysis of torque ripple and flux ripple. The proposed methods are simulated using MATLAB/SIMULINK and experimental response shows the validity of the developed methods.

1 Introduction

Variable frequency drives are a workhorse of industries, better performance of VFDs relies on dynamic response, simplicity, lesser ripple in torque and flux. These characteristics of VFDs attain an interesting area for researchers. VFDs are developed with field-oriented control (FOC) or direct torque control (DTC). The scheme of DTC circumvents the problems involved in FOC-like coordinate transformation. DTC provides most of the characteristics of VFDs and this was developed by Takahashi and Nogouchi [1]. DTC has limitations: the use of hysteresis controllers causes variable switching frequencies, start-up problems and complex look-up tables for multilevel inversion. Some of these limitations can be prevented by predictive torque control (PTC). The advantages offered by model predictive control are easy to control, implement, understand and addition of constraints in cost function. Due to their vast advantages, the combination of direct torque control and model predictive control leads to the implementation of PTC. An extensive research has been carried out during the past decade on PTC to reduce torque and flux ripples. Correa *et al.* [2] have used PI controller and predictive controller together to obtain high dynamic response with the help of multilevel space phasor modulation. It uses a dead-beat controller to calculate slip-angle of rotors. This offers an adorable small-signal operation for multilevel inverter-fed induction machines. A new PTC algorithm for induction motors implemented in [3] is based on immediate flux control. It does not account for the ripples in torque and flux but reduces the switching frequency.

In [4], a discrete-time model of induction motor was developed in terms of state-space equations for the prediction of stator flux and torque. This article utilises finite control set model predictive control (FCSMPC) for its implementation and provides a solution to prevent time delays for the prediction algorithm. In [5, 6] the concept, evaluation, implementation and analysis of model predictive torque control (MPTC) of induction motors were developed using extrapolation. PTC offers lesser ripple in torque and flux when compared with DTC. In DTC, the hysteresis bounds are responsible to generate a switching vector; the selection of voltage vector is an indirect process, whereas in PTC the selection of the voltage vector is direct and obtained from optimisation of cost function. A simple prediction model is implemented for DTC to compensate delay time [7].

In the recent trend, the branches of PTC extended towards the reduction of torque and flux ripples. The variable switching time point PTC algorithm was introduced in [8] because PTC introduces high current and torque ripples due to the switching frequency which are less than half of the sampling frequency compared with modulator-based approaches. To solve real-time problems, variable switching time point is introduced to PTC. The concept of duty-ratio control was added to PTC to reduce torque ripple but it requires high sampling frequencies. In [9], an improved MPTC with duty-cycle control was implemented to reduce torque and flux ripples by optimising active voltage vectors as well as their duration. In [10], generalised predictive torque control (GPTC) of induction motor drive is implemented to run over the difficulties of duty-ratio controlled MPTC by using two voltage vectors. GPTC reduces the torque ripple but the computational burden is accountable. Computational burden involved in a finite control set PTC is expensive and utilises all voltage vectors for the prediction of torque and flux. The computational burden involved in PTC is higher compared with DTC; to conquer this novel DTC is developed [11] to reduce switching frequency based on a look-up table. The predictions of voltage vectors are always dependent on two adjacent active vectors and a null vector.

In [12], a novel algorithm is proposed to control the torque of induction motor using the angle between rotor flux and stator current by developing the necessary equations for the prediction of torque. The developed equations of current and torque predictions are independent of voltage. In PTC, the optimisation of cost function is dependent on torque and flux weighting factors. Tuning of the weighting factor and selection of the weighting factor is tedious [13]. To circumvent this, PTC of induction motor was modified as model predictive flux control (MPFC) rather than MPTC and it uses a control variable stator flux to eliminate complex predictions. In [14], MPTC was developed by converting torque and flux in terms of equivalent voltage vectors to eliminate the effects of weighting factors on current and torque ripples. The branch and bound algorithm was used to find the weighting factor [15, 16]. Formulation of the flux weighting factor described in [15, 16] describes the formulation of weighting factor for common-mode voltage.

The prediction algorithm of PTC involves measurement of speed and currents. In [17], two sensorless PTC methods are introduced; these are voltage model observer and sliding mode observer. Direct estimation of speed from the current is possible but it degrades the steady-state performance. To circumvent this, extended Kalman filter (EKF) is used to estimate the speed by using flux and stator currents [18]. In [19], sensorless PTC of

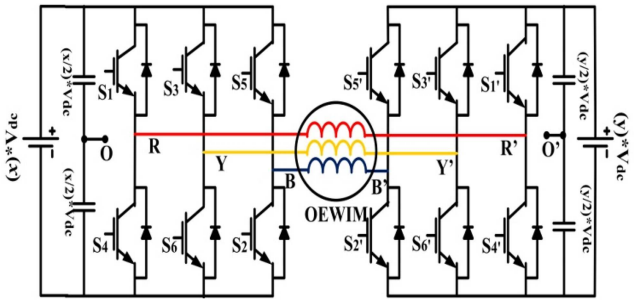

Fig. 1 *Power circuit of OEWIM*

induction motor was developed by estimating rotor speed and rotor flux with the help of EKF.

From the literature, PTC also suffers from variable switching frequencies, higher ripples in torque and flux. To curtail torque and flux ripples, it is better to use duty-cycle control or multilevel inverter-fed induction motor drives. The multilevel inversion with less number of switches can be obtained by using an open-end winding configuration. This is the motivating factor to implement PTC for open-end winding induction motors (OEWIMs). Dual-inverter-fed OEWIM is a better alternative for multilevel inversion schemes. OEWIM with dual-inverter configuration offers several advantages: (i) multilevel inversion from two two-level inverters; (ii) absence of clamping diodes as involved in neutal-point clamped (NPC) inverters; (iii) it offers high redundancy of switching states; (iv) less number of capacitors compared with flying capacitor multilevel inverters and (v) few number of DC sources when compared with cascaded H-bridge configuration [20].

OEWIM has several applications such as in hybrid electric vehicles (HEV) [21, 22], propulsion [23] and renewable energy systems [24–26]. OEWIM configuration is also extendible for more than four-level inversion by replacing two-level inverters with three-level NPC inverters [27]. In [28], DTC of OEWIM is implemented with '8' switching states to obtain two-level voltage. In [29], DTC of OEWIM is implemented with equal DC link voltages to obtain three-level output voltage using space vector modulation. In [30], DTC of induction motor was implemented with 3 two-level inverters in cascaded H-bridge mode but it needs 18 switches for its operation, whereas the OEWIM requires 12 switches for its operation to obtain four-level inversion. DTC of OEWIM for four-level inversion with space vector modulation is reported [31–33]. The calculation of reference voltage space vector and clamping of inverter to a particular switching state is complex. The problems involved in the implementation of DTC of OEWIM for multilevel inversion can be easily addressed by predictive torque control.

This article clearly describes the implementation of PTC for OEWIM drive. Intents of the article are: implementation of a discrete model of OEWIM, mathematical model of an inverter, formulating switching states and their classification. In this article, OEWIM is subjected to operate with two-level and multilevel inversion. By operating the two inverters with equal (1:1 ratio) DC link voltage, two-level and three-level output voltages can be obtained, whereas four-level output voltage can be obtained by operating the two inverters with unequal (2 : 1 ratio) DC link voltages. Hence, in this article the OEWIM drive is operated with two-, three- and four-level inversion schemes by classifying the voltage vectors according to the operating speed. The computational burden involved can be reduced by classifying the voltage vectors. A comparative study has been carried out on torque ripple for different inversion schemes. The proposed algorithms are implemented by using dSPACE DS-1104 controller board.

2 Inverter configuration and modelling of OEWIM

The configuration of OEWIM to obtain multilevel inversion is shown in Fig. 1. In the power circuit by operating two inverters with equal DC link voltages ($x = y = 1/2$), it is easy to obtain two- and three-level output voltages, whereas by operating the two inverters in the ratio of 2:1 ($x = 2/3$; $y = 1/3$), four-level output voltage can be obtained [34]. To obtain four-level inversion, VSI-1 is operated with a voltage of ($2V_{dc}/3$) and VSI-2 is operated with a voltage of ($V_{dc}/3$).

The pole voltages of VSI-1 and VSI-2 with reference to midpoint of the top and bottom capacitors are given by (1) and (2), whereas (3) shows the difference in pole voltages:

$$\begin{pmatrix} V_{ro} \\ V_{yo} \\ V_{bo} \end{pmatrix} = (x * V_{dc}) \begin{pmatrix} S_r \\ S_y \\ S_b \end{pmatrix} \tag{1}$$

$$\begin{pmatrix} V_{r'o'} \\ V_{y'o'} \\ V_{b'o'} \end{pmatrix} = (y * V_{dc}) \begin{pmatrix} S_{r'} \\ S_{y'} \\ S_{b'} \end{pmatrix} \tag{2}$$

$$\begin{pmatrix} \Delta V_{rr'} \\ \Delta V_{yy'} \\ \Delta V_{bb'} \end{pmatrix} = \begin{pmatrix} V_{ro} - V_{r'o'} \\ V_{yo} - V_{y'o'} \\ V_{bo} - V_{b'o'} \end{pmatrix} \tag{3}$$

From the difference of phase voltages the common-mode voltage can be written as (4) and phase voltages of OEWIM are given by (5)

$$V_{oo}' = V_o = \left(\frac{1}{3}\right)(\Delta V_{rr'} + \Delta V_{yy'} + \Delta V_{bb'}) \tag{4}$$

$$\begin{pmatrix} V_{rr'} \\ V_{yy'} \\ V_{bb'} \end{pmatrix} = \frac{1}{3} \begin{pmatrix} 2 & -1 & -1 \\ -1 & 2 & -1 \\ -1 & -1 & 2 \end{pmatrix} \begin{pmatrix} \Delta V_{rr'} \\ \Delta V_{yy'} \\ \Delta V_{bb'} \end{pmatrix} \tag{5}$$

2.1 Dynamic model of OEWIM

Fig. 2 describes the dynamic model of OEWIM in stationary reference frames. It clearly describes the operation of OEWIM for multilevel inversion. In block diagram V_{rr}', V_{yy}', and V_{bb}' are phase voltages and the dynamic equations of OEWIM are given by (6)–(11).

The stator and rotor voltages of OEWIM in stationary reference frames are given by

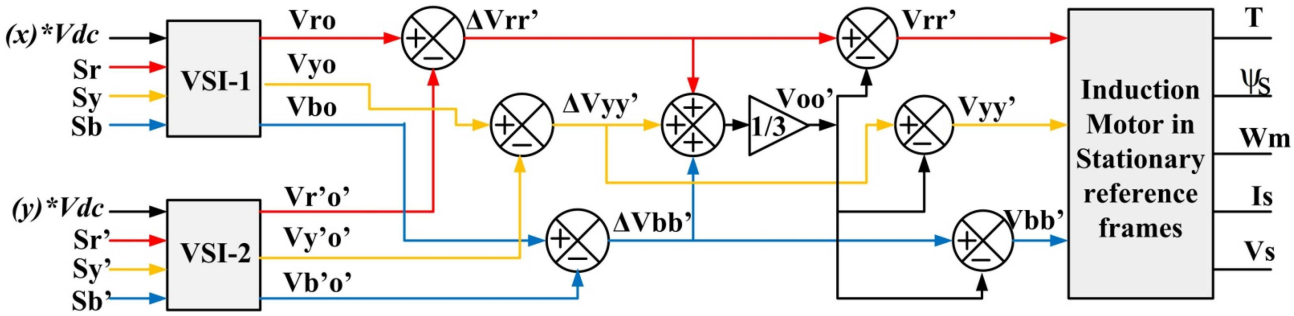

Fig. 2 *Common-mode voltage model and OEWIM configuration in stationary reference frames*

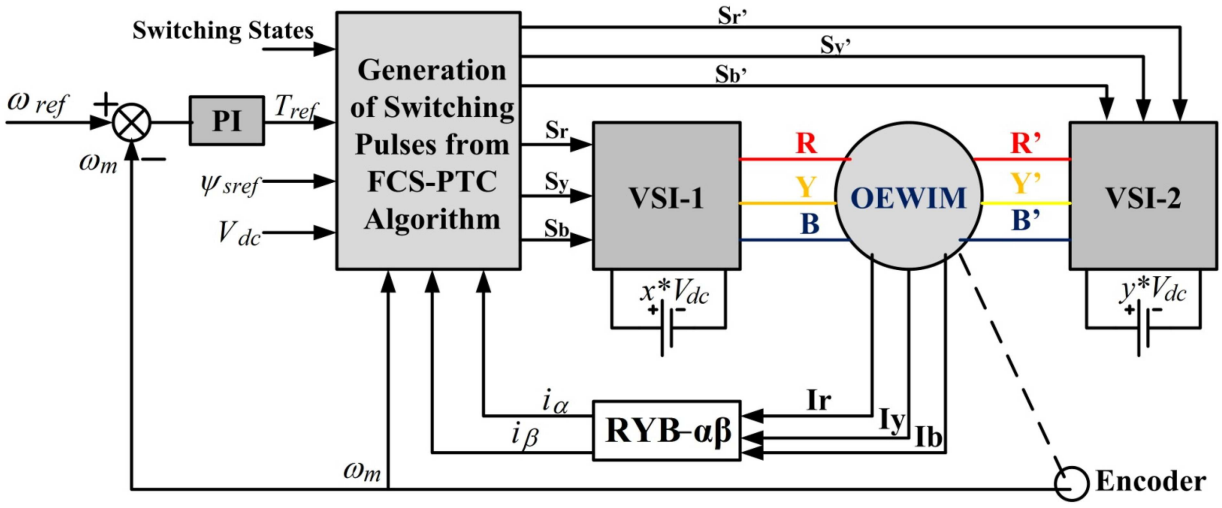

Fig. 3 *Proposed predictive torque control algorithm*

$$\begin{pmatrix} V_{s\alpha}(k) \\ V_{s\beta}(k) \end{pmatrix} = R_s \begin{pmatrix} i_{s\alpha}(k) \\ i_{s\beta}(k) \end{pmatrix} + \frac{d}{dt} \begin{pmatrix} \psi_{s\alpha}(k) \\ \psi_{s\beta}(k) \end{pmatrix} \tag{6}$$

$$\begin{pmatrix} 0 \\ 0 \end{pmatrix} = R_r \begin{pmatrix} i_{r\alpha}(k) \\ i_{r\beta}(k) \end{pmatrix} + \frac{d}{dt} \begin{pmatrix} \psi_{r\alpha}(k) \\ \psi_{r\beta}(k) \end{pmatrix} + \omega_r \begin{pmatrix} \psi_{r\beta}(k) \\ -\psi_{r\alpha}(k) \end{pmatrix} \tag{7}$$

The stator and rotor flux linkages of OEWIM are given by

$$\begin{pmatrix} \psi_{s\alpha}(k) \\ \psi_{s\beta}(k) \end{pmatrix} = L_s \begin{pmatrix} i_{s\alpha}(k) \\ i_{s\beta}(k) \end{pmatrix} + L_m \begin{pmatrix} i_{r\alpha}(k) \\ i_{r\beta}(k) \end{pmatrix} \tag{8}$$

$$\begin{pmatrix} \psi_{r\alpha}(k) \\ \psi_{r\beta}(k) \end{pmatrix} = L_r \begin{pmatrix} i_{r\alpha}(k) \\ i_{r\beta}(k) \end{pmatrix} + L_m \begin{pmatrix} i_{s\alpha}(k) \\ i_{s\beta}(k) \end{pmatrix} \tag{9}$$

From (6) to (9), the torque of the motor drive is given by (10); the speed of OEWIM can be obtained from its mechanical equation shown in (11):

$$T(k) = \left(\frac{3}{2}\right)\left(\frac{P}{2}\right)\left(\psi_{s\alpha}(k) i_{s\beta}(k) - \psi_{s\beta}(k) i_{s\alpha}(k)\right) \tag{10}$$

$$J\frac{d\omega_m}{dt} = T - T_l \tag{11}$$

3 The Proposed PTC strategy

The block diagram of the proposed PTC is shown in Fig. 3. In this article, the PTC algorithm for OEWIM was divided into three modes based on output voltage from the inverter; Mode-1: two-level output voltage, Mode-2: three-level output voltage and Mode-3: four-level output voltage. The locations of active voltage space vectors for multilevel inversion can be obtained by using (12)–(14):

$$V_{s1} = \left(\frac{2}{3}\right)(x * V_{dc})\left(S_r + S_y e^{j2\pi/3} + S_b e^{j4\pi/3}\right) \tag{12}$$

$$V_{s2} = \left(\frac{2}{3}\right)(y * V_{dc})\left(S_r' + S_y' e^{j2\pi/3} + S_b' e^{j4\pi/3}\right) \tag{13}$$

The resultant voltage space vector (14) is obtained from the difference of (12) and (13):

$$V_s = V_{s1} - V_{s2} \tag{14}$$

'V_{s1}'and 'V_{s2}' are the output voltages of inverter-1 and inverter-2.

The resultant voltage space vector (V_s) is obtained from realisation (14) of all possible switching states of VSI-1 and VSI-2. The switching states are realised by using $S_r = S_y = S_b = S_r' = S_y' = S_b' = 1/0$. '1' indicates upper switch in the respective leg is ON. '0' indicates a lower switch in the respective leg is ON. OEWIM drive with a dual-inverter configuration is rich in redundancy of switching states [20] and offers 64 switching combinations; out of these combinations it offers 37 locations for four-level inversion, 18 locations for three-level inversion and 7 locations for two-level inversion. The switching states and location of active voltage vector locations for the two-level inversion are clearly described [28].

Locations of voltage space vectors are obtained from the switching states of the VSI-1 and VSI-2. If VSI-1 and VSI-2 are operated with equal DC link voltages (i.e. $x = y = 1/2$), then it gives two-level (7 space vector locations) and three-level (18 space vector locations) output voltage, whereas four-level output voltage can be obtained by operating the inverters with unequal DC link voltages (i.e. $x = 2/3$; $y = 1/3$). The locations of active voltage space vectors are shown in Figs. 4*a–c* for two-level, three-level and four-level inversion. In the classical DTC of induction motors, it requires a three-level torque hysteresis controller, if it is desired to operate an induction motor in a four-level inversion it requires multi-level hysteresis controllers and modification of the look-up table. The selection of the voltage vector depends on hysteresis boundaries, which may cause higher ripple in torque and flux [35, 36]. To circumvent this problem and to operate induction motor with multilevel inversion, OEWIM is a better alternative to meet the features of VFDs. In the proposed PTC strategy, the voltage space vector locations are classified into various groups and the selection of active voltage vector is from optimisation of cost function. In PTC, the selection of active voltage vector is direct and chooses the voltage vector to reduce torque and flux ripple. In case of two-level inversion mode, there are seven space vector locations; the computational burden involved in this mode is less when compared with three- and four-level inversion modes. In the three-level inversion mode, the voltage space vector has 18 locations; locations V_1 to V_6 are used for speeds less than 50% of the rated speed, whereas the active vector locations V_7 to V_{18} are used for speeds more than 50% of the rated speed. In four-level inversion, the active voltage space vector has 36 locations; locations V_1 to V_6 are used for speeds less than 35% of the rated speed; locations V_7 to V_{18} are used for speeds between 35% of the rated speed and 70% of the rated speed and locations V_{19} to V_{36} are used for speeds more than 70% of rated speed. For multilevel inversion, PTC involves large computational burden, to abate this problem, the voltage space vector is classified into various categories.

Once the switching states and their realisations are calculated, then it is easy to predict torque and flux of an open-end winding induction motor drive.

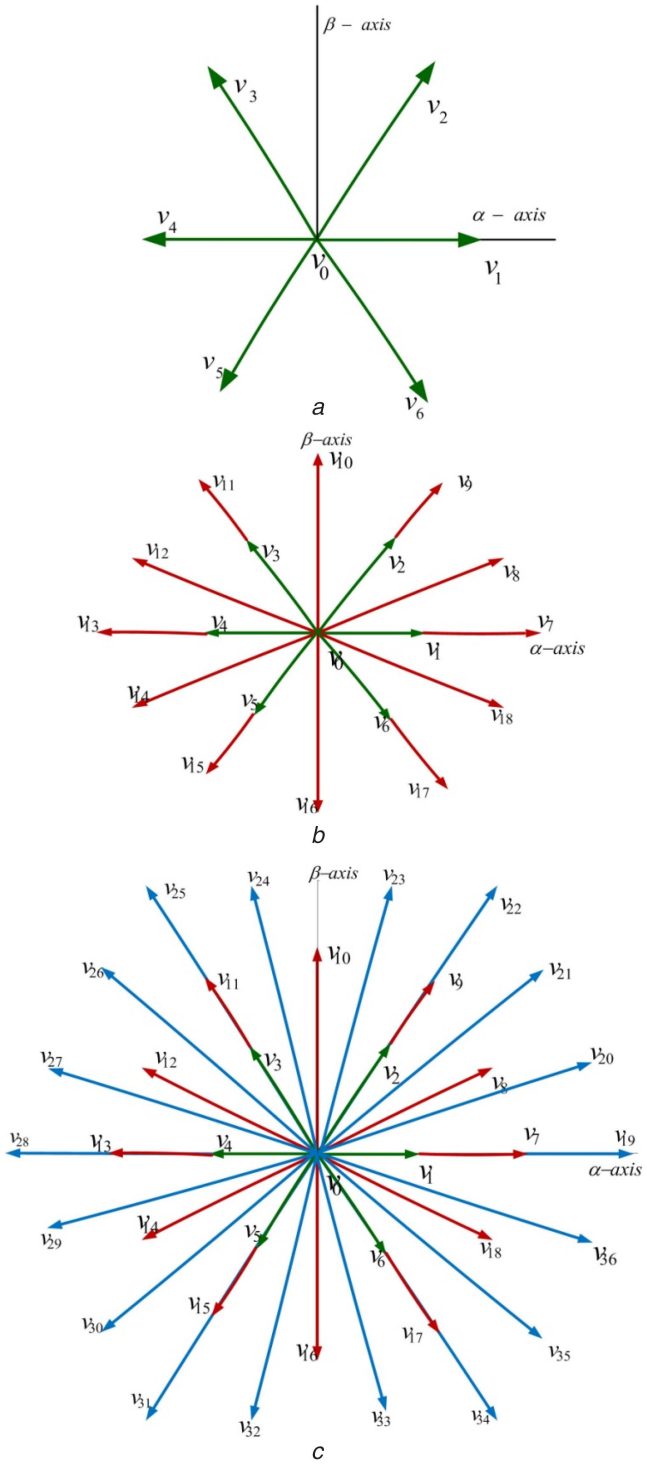

Fig. 4 *Location of voltage space vectors*
(a) Two-level inversion, ***(b)*** Three-level inversion and, ***(c)*** Four-level inversion

3.1 Prediction algorithm

The concept of PTC depends on measurements, estimation and prediction of behaviour of the OEWIM in the next control cycle. In the previous section, the discrete model of OEWIM was shown in stationary reference frames at the kth instance; for the prediction of torque and flux at the $(k+1)$th instance, it requires speed and current measurements. If currents are measured, then by using stator voltage, flux linkages of stator (15) and flux linkages of rotor (16) can be estimated. The predicted values of torque and flux are obtained from the measurements and estimations at the kth instance:

$$\frac{\mathrm{d}}{\mathrm{d}t}\begin{pmatrix}\psi_{s\alpha}(k)\\ \psi_{s\beta}(k)\end{pmatrix} = R_s\begin{pmatrix}i_{s\alpha}(k)\\ i_{s\beta}(k)\end{pmatrix} - \begin{pmatrix}V_{s\alpha}(k)\\ V_{s\beta}(k)\end{pmatrix} \tag{15}$$

$$\begin{pmatrix}\psi_{r\alpha}(k)\\ \psi_{r\beta}(k)\end{pmatrix} = A\begin{pmatrix}\psi_{s\alpha}(k)\\ \psi_{s\beta}(k)\end{pmatrix} + B\begin{pmatrix}i_{s\alpha}(k)\\ i_{s\beta}(k)\end{pmatrix} \tag{16}$$

The predictions of torque and flux are developed by using the forward Euler's approach [37] and it is shown in (17):

$$\frac{\mathrm{d}F}{\mathrm{d}t} = \frac{F(k+1)-F(k)}{T_s} \tag{17}$$

Therefore, from (17) the next state can be predicted as

$$F(k+1) = \frac{\mathrm{d}F}{\mathrm{d}t}T_s + F(k) \tag{18}$$

From (15) and (18)

$$\begin{pmatrix}\psi_{s\alpha}(k+1)\\ \psi_{s\beta}(k+1)\end{pmatrix} = T_s\left(\begin{pmatrix}V_{s\alpha}(k)\\ V_{s\beta}(k)\end{pmatrix} - R_s\begin{pmatrix}i_{s\alpha}(k)\\ i_{s\beta}(k)\end{pmatrix}\right) + \begin{pmatrix}\psi_{s\alpha}(k)\\ \psi_{s\beta}(k)\end{pmatrix} \tag{19}$$

$$\begin{pmatrix}i_{s\alpha}(k+1)\\ i_{s\beta}(k+1)\end{pmatrix} = T_s\left(E\begin{pmatrix}\psi_{r\alpha}(k)\\ \psi_{r\beta}(k)\end{pmatrix} - F\begin{pmatrix}i_{s\alpha}(k)\\ i_{s\beta}(k)\end{pmatrix} + G\begin{pmatrix}\psi_{r\beta}(k)\\ -\psi_{r\alpha}(k)\end{pmatrix} + \frac{1}{D}\begin{pmatrix}V_{s\alpha}(k)\\ V_{s\beta}(k)\end{pmatrix}\right) + \begin{pmatrix}i_{s\alpha}(k)\\ i_{s\beta}(k)\end{pmatrix} \tag{20}$$

$$T(k+1) = \left(\frac{3}{2}\right)\left(\frac{P}{2}\right)\left(\psi_{s\alpha}(k+1)i_{s\beta}(k+1) - \psi_{s\beta}(k+1)i_{s\alpha}(k+1)\right) \tag{21}$$

where
$A = L_r/L_m, B = (L_m - L_sL_r/L_m), C = (L_mR_r/L_r), D = \left(L_sL_r - L_m^2/L_r\right),$
$E = \left(L_mR_r/L_r^2D\right), F = L_m/L_rD((L_mR_r/L_r) + (R_sL_r/L_m))$
and $G = (L_m/L_rD)$.

3.2 Formulation of cost function

To obtain the switching states of an inverter, optimisation of cost function is required. The prerequisites of cost function are common-mode voltage (V_o), stator flux reference (ψ_{sref}), predicted values of stator flux (ψ_s $(k+1)$), torque reference (T_{ref}) and predicted value of electromagnetic torque (T_{k+1}). The cost function of the proposed PTC is shown in

$$g = \sigma_T(T_{ref} - T_{k+1}) + \sigma_\psi(\psi_{sref} - \psi_s(k+1)) + \sigma_n(V_o) \tag{22}$$

The cost function (22) should be optimised for each active voltage state of OEWIM drive configuration. The optimisation of cost functions in such a way that the selected stator voltage vector can produce fewer ripples in torque, flux and less common-mode voltage. In (22), σ_T, σ_ψ and σ_n are the weighting factors of torque, flux and common-mode voltage. The weighting factors used for simulation and experiment are $\sigma_T = 1, \sigma_\psi = 75$ and $\sigma_n = 0.1$. Branch and bound algorithm is used to determine the weighting factors and they are obtained from several offline simulations. The procedure to find the weighting factors for common-mode voltage and stator flux is reported [15, 16]. In [15], the procedure to select stator flux weighting factor and its effect on the performance of induction motor drive are presented. The selection of weighting factor for common-mode voltage and its influence on current is reported [16].

4 Results and discussions

The proposed PTC of OEWIM is shown in Fig. 3, to validate the proposed algorithm it is simulated using MATLAB and verified experimentally by using dSPACE DS-1104 controller board. VSIs are used in OEWIM drive operated with DC link voltages of 270 and 270 V, respectively, for two- and three-level inversion schemes; therefore the effective DC link voltage is 540 V. For four-level inversion, VSI-1 and VSI-2 are operated with DC link voltages of 360 and 180 V with an effective DC link voltage of 540 V.

Table 1 Specifications of OEWIM

Name	Symbol	Quantity
stator resistance	R_s	4.2 Ω
rotor resistance	R_r	2.6794 Ω
stator inductance	L_s	0.54 H
rotor inductance	L_r	0.54 H
mutual inductance	L_m	0.512 H
poles	P	4
inertia	J	0.031 kg/m^2
power	P	3.7 kW
nominal torque	T	24.48 N m
nominal flux	ψ	1 Wb
nominal speed	N_r	1440 RPM

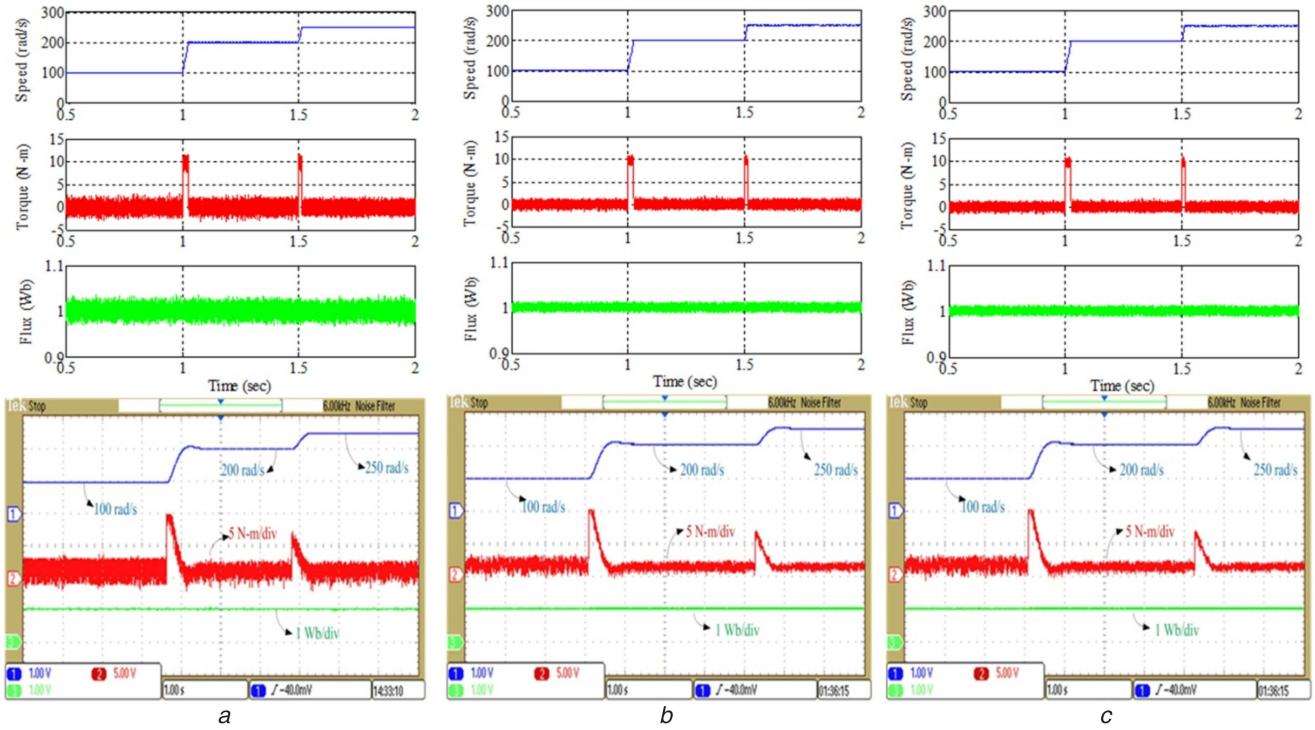

Fig. 5 *Speed, torque and flux in forward motoring of OEWIM drive for 100, 200 and 250 rad/s*

(a) Simulated and experimental response for two-level inversion, ***(b)*** simulated and experimental response for three-level inversion, ***(c)***simulated and experimental response for four-level inversion

To verify the proposed PTC algorithms, the OEWIM drive is subjected to operate at various speeds; for brevity, the simulation and experimental results are shown for 100, 200 and 250 rad/s in both forward and reverse motoring modes. The parameters of OEWIM drive used for the verification of experimental response are given in Table 1. The test bench used for verification of the proposed algorithms is described in the Appendix. The focus of this article is to develop PTC for OEWIM drive with equal and unequal DC link voltages and also to show the simulation and experimental response for three inversion schemes.

It is a well-known fact that by operating induction motor drives with multilevel output voltages, the torque ripple and flux ripple decrease. A comparison of two-level, three-level and four-level inversion schemes with the PTC algorithm was presented with simulation and experimental results. The OEWIM was tested under no-load condition; therefore the reference torque is zero in the steady-state condition and the nominal/reference flux is 1 Wb. Torque ripple and flux ripple are estimated from the deviation of actual values of torque (10) and flux (8) with respect to reference torque and flux.

Figs. 5–11 shows the simulated and experimental response of OEWIM drive for various speeds. For step change of speed response from 100, 200 and 250 rad/s are shown in Fig. 5 for two-level, three-level and four-level inversion, respectively, in forward motoring. From Fig. 5, it can be observed that if motor drive is operating with multilevel output voltage fed by an inverter, then it gives reduced ripple in torque and flux.

Fig. 6 shows the simulated and experimental response of OEWIM drive in reverse motoring mode for step change in speed. Fig. 6 gives variation of torque and flux ripple for different output voltage levels of an inverter and it gives higher ripple in torque and flux at −100 rad/s as the speed of the motor drive increases the input voltage to its stator terminals may increase and gives reduced ripple in torque and flux at −200 and −250 rad/s. Fig. 6*a* is simulated and experimental response of OEWIM drive in reverse motoring for two-level inversion, whereas Figs. 6*b* and *c* represent simulated and experimental response of OEWIM for three-level and four-level inversion.

Simulated and experimental response of torque and flux of OEWIM drive for a step change in speed from 200 rad/s to −200 rad/s is shown in Fig. 7 for two, three and four-level inversion respectively. From Fig. 7, torque and flux ripple reduces for four-level inversion when compared with two- and three-level inversion. Fig. 7 also illustrates that the settling time required for a four-level inversion is less when compared with two- and three-level inversion.

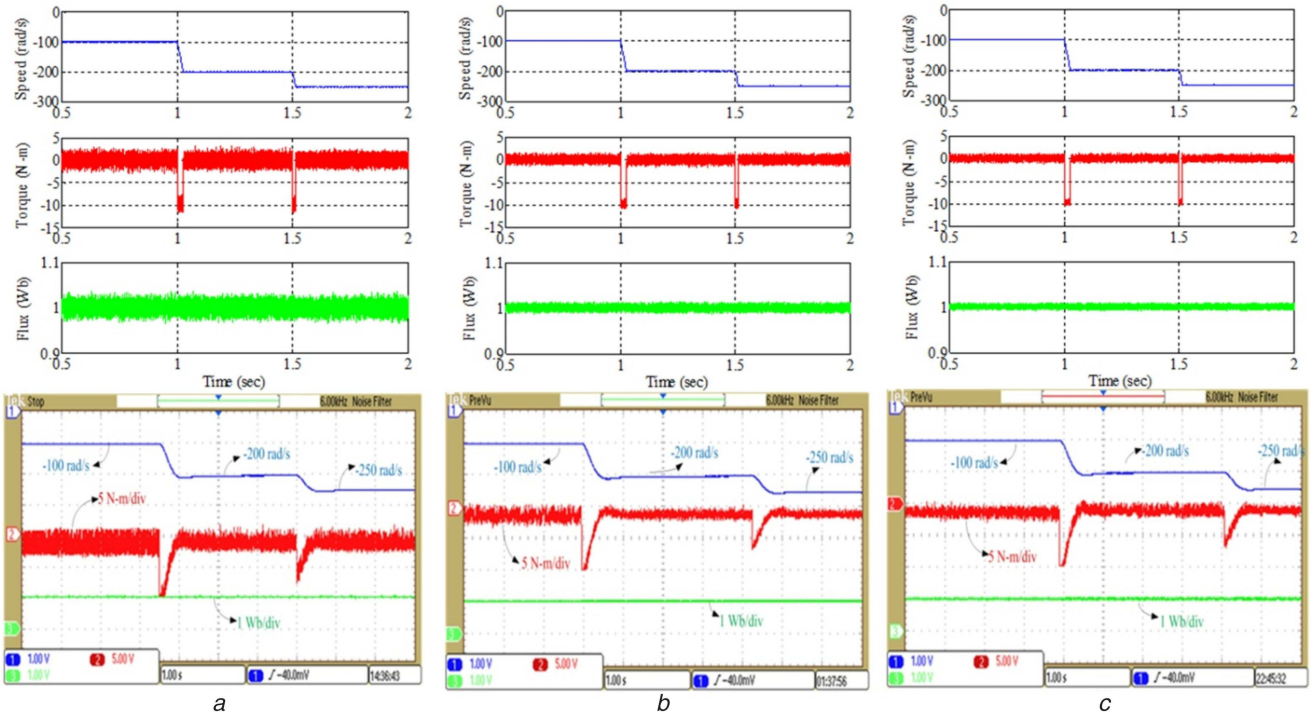

Fig. 6 *Speed, torque and flux in reverse motoring of OEWIM drive for −100, −200 and −250 rad/s*

(a) Simulated response and experimental response for two-level inversion, ***(b)*** simulated and experimental response of three-level inversion and, ***(c)*** simulated and experimental response for four-level inversion

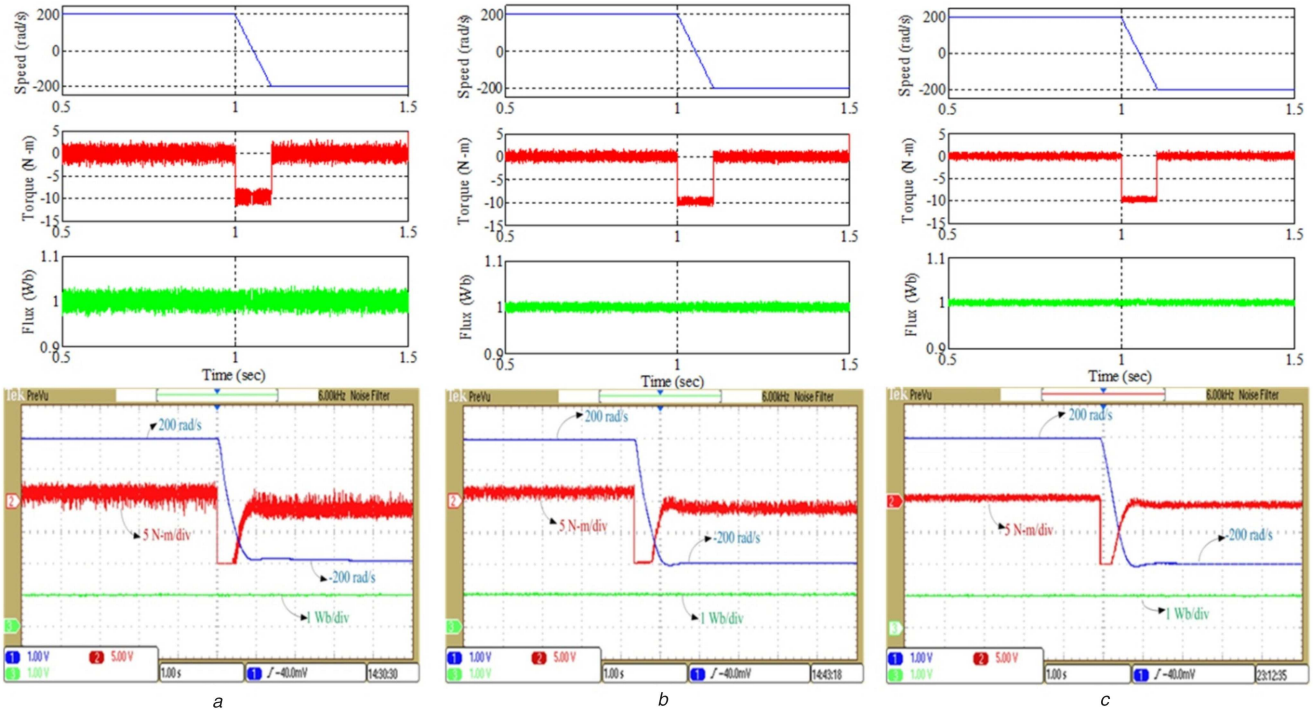

Fig. 7 *Speed, torque and flux in forward to reverse motoring of OEWIM drive for 200 to −200 rad/s*

(a) Simulated and experimental response for two-level inversion, ***(b)*** simulated and experimental response of three-level inversion, ***(c)*** simulated and experimental response of four-level inversion

Fig. 8 shows the simulated and experimental response of speed, current and voltage of OEWIM drive in forward motoring at a speed of 250 rad/s. Fig. 8*a* gives simulated and experimental response of OEWIM drive for a speed of 250 rad/s in forward motoring for two-level inversion, whereas Figs. 8*b* and *c* represent simulated and experimental response of OEWIM drive for a speed of 250 rad/s in forward motoring for three- and four-level inversion, respectively. Fig. 9 shows simulated and experimental response of speed, voltage and common-mode voltage of OEWIM drive at a speed of 200 rad/s; the common-mode voltage may vary for different values for weighting factor, for a fair comparison it is taken as constant for the three cases.

Fig. 9*a* shows the speed, voltage and common-mode voltage of OEWIM drive for a speed of 200 rad/s in forward motoring for two-level inversion, whereas Figs. 9*b* and *c* represent the simulated and experimental response for three- and four-level inversion schemes.

From Fig. 9, it is evident that by operating OEWIM with three- and four-level inversion, the common-mode voltage can be reduced. In the cost function of the proposed algorithm, the

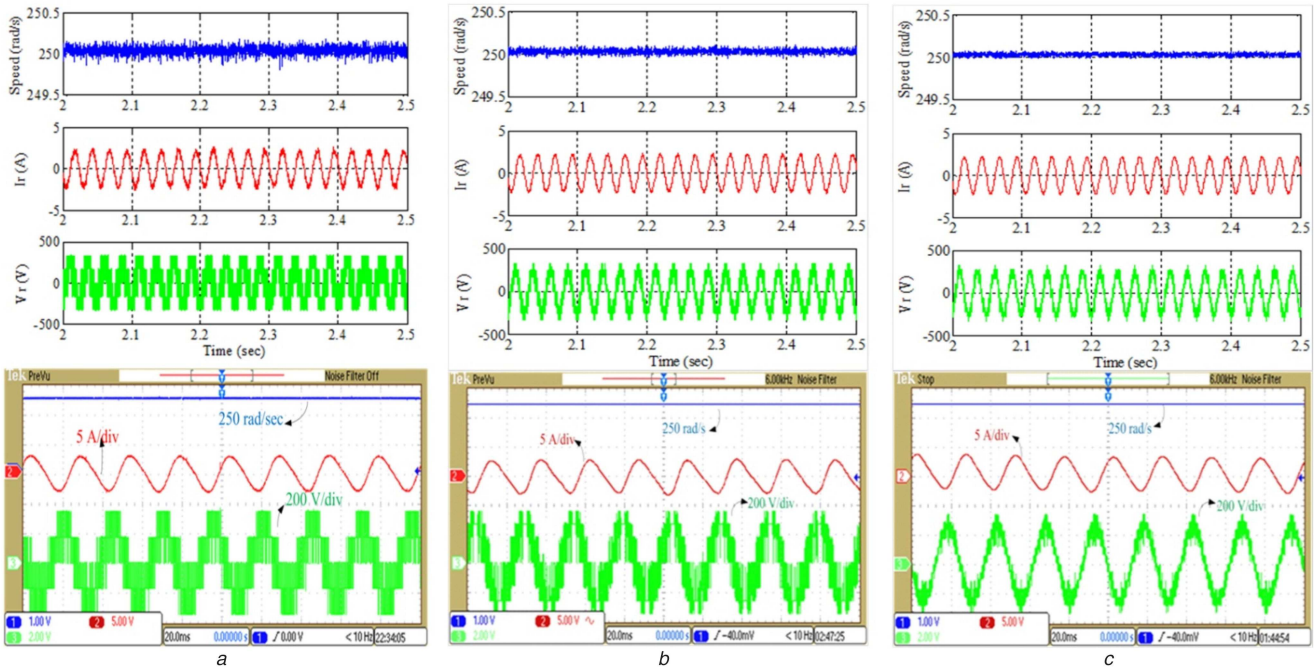

Fig. 8 *Speed, current and voltage of OEWIM drive*

(a) Simulated and experimental response for two-level inversion, ***(b)*** simulated and experimental response of three-level inversion, ***(c)*** simulated and experimental response of four-level inversion

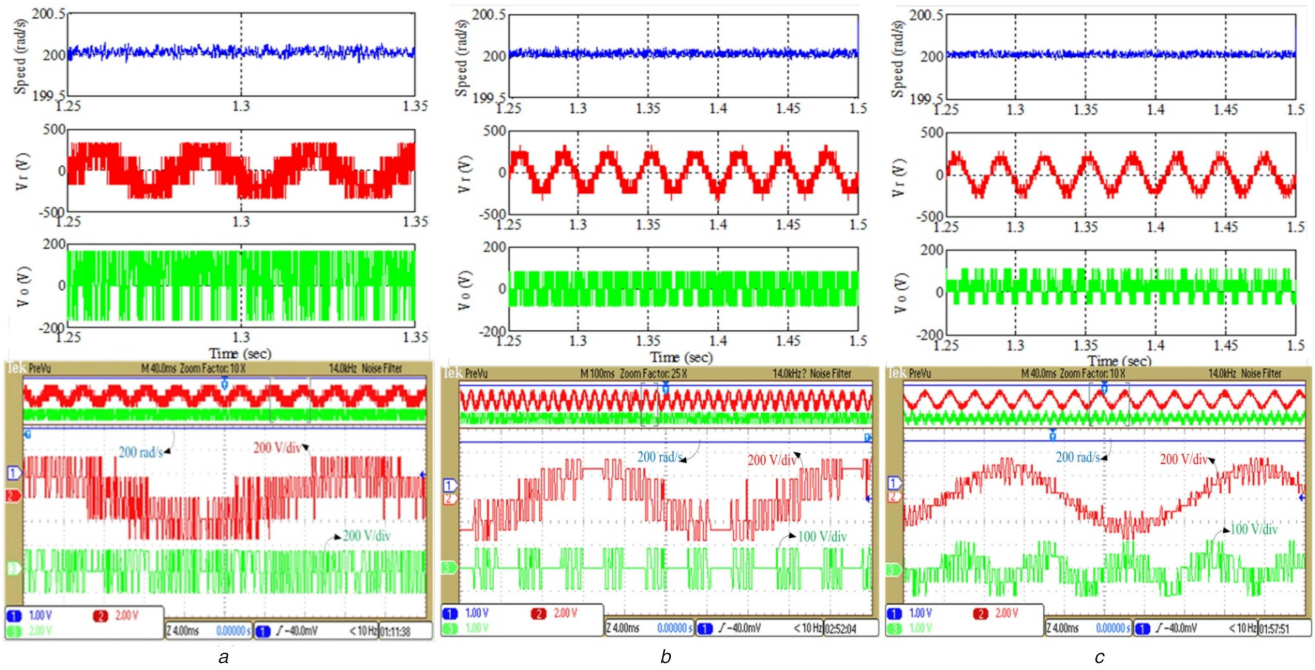

Fig. 9 *Speed, voltage and common-mode voltage of OEWIM drive*

(a) Simulated and experimental response for two-level inversion, ***(b)*** simulated and experimental response of three-level inversion, ***(c)*** simulated and experimental response of four-level inversion

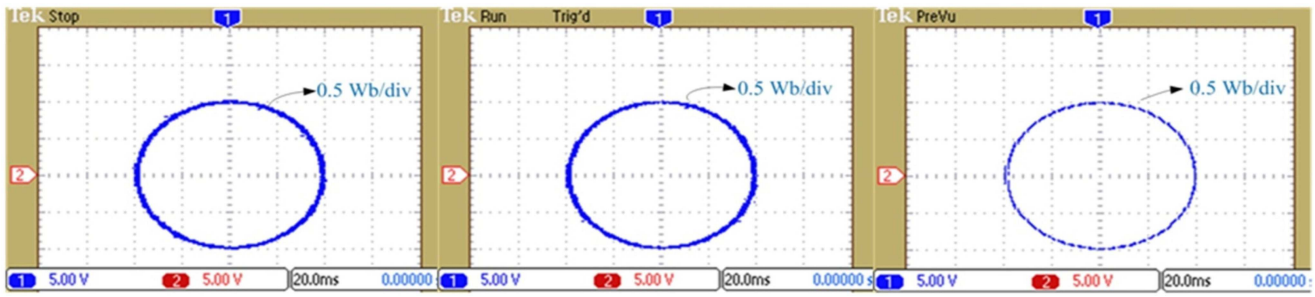

Fig. 10 *Flux locus of OEWIM drive for two-, three- and four-level inversion, respectively*

Table 2 Experimental steady-state torque and flux ripple of OEWIM drive for different operating speeds

Control Algorithm	Speed (rad/s)	2-level inversion		3-level inversion		4-level inversion	
		Torque ripple (N-m)	Flux ripple (Wb)	Torque ripple (N-m)	Flux ripple (Wb)	Torque ripple (N-m)	Flux ripple (Wb)
DTC	100	4.5	0.057	4.1	0.048	3.4	0.038
Proposed PTC		3.8	0.032	3.2	0.028	2.8	0.025
DTC	200	3.3	0.045	3	0.038	2.8	0.03
Proposed PTC		2.8	0.02	2.5	0.018	2	0.016
DTC	250	2.5	0.035	2.25	0.028	1.85	0.025
Proposed PTC		2	0.013	1.75	0.0125	1.4	0.01

common-mode voltage is added, by adding this term into cost function the switching states are chosen accordingly for minimum values of common-mode voltage. Therefore, the effect of common-mode voltage is reduced from two-level inversion to a four-level inversion.

From Figs. 5–7, it is clear that the torque and flux ripples decrease by using a multilevel inversion scheme. To reduce the computational burden on the controller, the voltage vectors have been classified into different groups, whereas for two-level inversion or in the case of classical PTC, there are six active voltage vectors and two null vectors. Therefore, for two-level inversion and classical PTC, the six active voltage vectors are applied for all speed ranges, whereas in the proposed three-level and four-level inversion schemes the voltage vectors are classified to operate based on input reference speed; therefore the classification active voltage vectors not only reduces torque and flux ripple but also effects the computational burden on converters.

Fig. 10 illustrates flux loci of OEWIM for two-, three- and four-level inversion. Flux locus is obtained by estimating α-axis and β-axis flux with a simple flux observer. By integrating (15), real and imaginary components of flux are estimated. From Fig. 10*c*, it is seen that the flux ripple is less when compared with two- and three-level inversion. The steady-state torque and flux ripple of OEWIM drive for various speeds of operation is listed in Table 2. The proposed PTC algorithms develop lesser ripple in torque and flux when compared with classical DTC for OEWIM configuration.

5 Conclusion

This article develops the scheme of PTC for OEWIM drive using equal and unequal DC link voltages. It clearly describes implementation, mathematical modelling and analysis of PTC and impact of classification of voltage vectors on speed, torque and flux. To reduce complexity and computational burden one step ahead prediction (prediction horizon $N = 1$) is performed. The proposed algorithm is simple and extendable for more than four-level inversion by replacing two-level inverters with three-level NPC inverters. For three-level and four-level inversion, the computational burden is high; the burden can be reduced by classifying the voltage vectors. By using the OEWIM drive, it is easy to implement PTC with reduced torque and flux ripples for multilevel inversion. The simulation and experimental results show the effectiveness of the proposed PTC algorithms and give better steady-state response for multilevel inversion.

6 References

[1] Takahashi, I, Noguchi, T.: 'A new quick-response and high efficiency control strategy of an induction motor', *IEEE Trans. Ind. Appl.*, 1986, **22**, (5), pp. 820–827

[2] Correa, P., Pacas, M., Rodriguez, J.: 'Predictive torque control for inverter-Fed induction machines', *IEEE Trans. Ind. Electron.*, 2007, **54**, (2), pp. 1073–1079

[3] Nemec, M., Nedeljkovic, D., Ambrozic, V.: 'Predictive torque control of induction machines using immediate flux control', *IEEE Trans. Ind. Electron.*, 2007, **54**, (4), pp. 2009–2017

[4] Miranda, H., Cortés, P., Yuz, J.I.*, et al.*: 'Predictive torque control of induction machines based on state-Space models', *IEEE Trans. Ind. Electron.*, 2009, **56**, (6), pp. 1916–1924

[5] Geyer, T., Papafotiou, G., Morrari, M.: 'Model predictive direct torque control—part I: concept, algorithm and analysis', *IEEE Trans. Ind. Electron.*, 2009, **56**, (6), pp. 1894–1905

[6] Papafotiou, G., Kley, J., Papadopoulos, K.G.*, et al.*: 'Model predictive direct torque control—part II: implementation and experimental evaluation', *IEEE Trans. Ind. Electron.*, 2009, **56**, (6), pp. 1906–1915

[7] Beerten, J., Verveckken, J., Driesen, J.: 'Predictive direct torque control for flux and torque ripple reduction', *IEEE Trans. Ind. Electron.*, 2010, **57**, (1), pp. 404–412

[8] Karamanakos, P., Stolze, P., Kennel, R.M.*, et al.*: 'Variable switching point predictive torque control of induction machines', *IEEE J. Emerg. Selc. Top. Power Electron.*, 2014, **2**, (2), pp. 285–295

[9] Zhang, Y., Yang, H.: 'Model predictive torque control of induction motor drives with optimal duty cycle control', *IEEE Trans. Power Electron.*, 2014, **29**, (12), pp. 6593–6603

[10] Zhang, Y., Yang, H.: 'Generalized Two-Vector-Based model-Predictive torque control of induction motor drives', *IEEE Trans. Power Electron.*, 2015, **30**, (7), pp. 3818–3829

[11] Habibullah, Md., Dah-Chuan Lu, D., Fazlur Rahman, Md.: 'A simplified finite-State predictive direct torque control for induction motor drive', *IEEE Trans. Ind. Electron.*, 2016, **63**, (6), pp. 3964–3975

[12] Alireza Davari, S.: 'Predictive direct angle control of induction motor', *IEEE Trans. Ind. Electron.*, 2016, **63**, (8), pp. 5276–5284

[13] Zhang, Y., Yang, H., Xia, B.: 'Model-predictive control of induction motor drives: torque control versus flux control', *IEEE Trans. Ind. Appl.*, 2016, **52**, (5), pp. 4050–4060

[14] Zhang, Y., Yang, H.: 'Two-Vector-Based model predictive torque control without weighting factors for induction motor drives', *IEEE Trans. Power Electron.*, 2016, **31**, (2), pp. 1381–1390

[15] Vargas, R., Ammann, U., Rodriguez, J.*, et al.*: 'Predictive strategy to control common-mode voltage in loads fed by matrix converters', *IEEE Trans. Ind. Electron.*, 2008, **55**, (12), pp. 4372–4380

[16] Rodriguez, J., Pontt, J., Silva, C.*, et al.*: 'Predictive direct torque control of an induction machine'. Proc. Conf. EPE-PEMC 2004 (Power Electronics and Motion control Conf.), Riga, Lativa, September 2004

[17] Alireza Davari, S., Arab Khaburi, D., Wang, F.*, et al.*: 'Using full order and reduced order observers for robust sensorless predictive torque control of induction motors', *IEEE Trans. Power Electron.*, 2012, **27**, (7), pp. 3424–3433

[18] Habibullah, Md., Dah-Chuan Lu, D.: 'A speed-Sensorless FS-PTC of induction motors using extended kalman filters', *IEEE Trans. Ind. Electron.*, 2015, **62**, (11), pp. 6765–6778

[19] Habibullah, Md., Dah-Chuan Lu, D., Xiao, D.*, et al.*: 'Predictive torque control of induction motor sensor-less drive Fed by a 3L-NPC inverter', *IEEE Trans. Ind. Inf.*, 2017, **13**, (1), pp. 60–70

[20] Somasekhar, V.T., Shivakumar, E.G., Gopakumar, K.*, et al.*: 'Multi level voltage space phasor generation for an open-end winding induction motor drive using a dual inverter scheme with asymmetrical DC-link voltages', *Eur. Power Electron. Drives J.*, 2002, **12**, (3), pp. 21–29

[21] Subotic, I., Bodo, N., Levi, E.*, et al.*: 'On-board integrated battery charger for EVs using an asymmetrical nine-phase machine', *IEEE Trans. Ind. Electron.*, 2015, **62**, (5), pp. 3285–3295

[22] Dehghani Kiadehi, A., El Khamlichi Drissi, K., Pasquier, C.: 'Angular modulation of dual-inverter fed open-end motor for electrical vehicle applications', *IEEE Trans. Power Electron.*, 2016, **31**, (4), pp. 2980–2990

[23] Lu, S., Corzine, K.: 'Multilevel multi-phase propulsion drives'.Proc. Conf. IEEE Electric Ship Technologies Symposium (ESTS), Philadelphia, PA, July 2005, pp. 363–370

[24] Kawabata, Y., Nasu, M., Nomoto, T.,, *et al.*: 'High-efficiency and low acoustic noise drive system using open winding AC motor and two space-vector modulated inverters', *IEEE Trans. Ind. Electron.*, 2002, **49**, (4), pp. 783–789
[25] Fernao Pires, V., Martins, J.F., Hao, C.: 'Dual-inverter for grid connected photovoltaic system: modeling and sliding mode control', *Sol. Energy*, 2012, **86**, (7), pp. 2106–2115
[26] Jain, S., Ramulu, C., Padmanadhan, S.,, *et al.*: 'Dual MPPT algorithm for dual PV source fed open-end winding induction motor drive for pumping application', *Eng. Sci. Technol. Int. J.*, 2016, **19**, (4), pp. 1771–1780
[27] Venugopal Reddy, B., Somasekhar, V.T., Kalyan, Y.: 'Decoupled space-vector PWM strategies for a four- level asymmetrical open-End winding induction motor drive with waveform symmetries', *IEEE Trans. Ind. Electron.*, 2011, **58**, (11), pp. 5130–5141
[28] Praveen Kumar, K.V., Vinay Kumar, T.: 'Experimental implementation of direct torque control of open-end winding induction motor'. Proc. Conf. IEEE TENCON-2016, pp. 3318–3323
[29] Kumar, A., Fernandes, B.G., Chatterjee, K.: 'Direct torque control of open-end winding induction motor drive using the concept of imaginary switching times for marine propulsion systems'. Proc. Conf. IEEE PESC-04, vol. **2**, pp. 1214–1219
[30] Vinay Kumar, T., Rao, S.S.: 'Direct torque controlled induction motor drive based on cascaded three two-Level inverters', *Int. J. Modell. Simul.*, 2014, **34**, (2), pp. 70–82
[31] Wu, D., Wu, X., Su, L.,, *et al.*: 'A dual three-level inverter based open-end winding induction motor drive with averaged zero-sequence voltage elimination and neutral-point voltage balance', *IEEE Trans. Ind. Electron.*, 2016, **63**, (8), pp. 4783–4795
[32] Satheesh, G., Brahmananda Reddy, T., Sai babu, C.H..: 'Four level decoupled SVPWM based direct torque control (DTC) of open end induction motor drive'. Proc. Conf. IEEE APCET-2012, vol. **2**, pp. 1–5
[33] Khairi Rahim, M., Patkar, F., Jidin, A.,, *et al.*: 'Reduced torque ripple and switching frequency using optimal DTC switching strategy for open-end winding of induction machines'. Proc. Conf. Power Electronics and Drive Systems (PEDS) 2015, 2015, pp. 767–772
[34] Suresh, L., Nagarjun, S., Somasekhar, V.T.: 'Improvised SVPWM strategies for an enhanced performance for a four-level open-end winding induction motor drive', *IEEE Trans. Ind. Electron.*, 2017, **64**, (4), pp. 2750–2759
[35] Buja, G.S., Kazmierkowski, M.P.: 'Direct torque control of PWM inverter-fed AC motors – a survey', *IEEE Trans. Ind. Electron.*, 2004, **51**, (4), pp. 744–757
[36] Vas, P.: '*Sensorless vector and direct torque control*' (Oxford University Press, New York, Yokyo, 1998)
[37] Rodriguez, J., Cortes, P.: '*Predictive control of power converters and electrical drives*' (John Wiley & Sons, Ltd., Chichester, United Kingdom, 2012)

7 Appendix

7.1 Experimental set-up

Test bench to verify the proposed algorithm for experimentation is shown in Fig. 11. The test bench contains a four-pole open-end winding induction motor, two two-level voltage source inverters, dSPACE DS-1104 controller board to deliver switching pulses, voltage and current transducers. MATLAB/SIMULINK RTI model is used to interface the dSPACE DS-1104 controller board.

Fig. 11 *Test bench used for experimentation*